Sodium-Ion Batteries

Deutsche Ausgabe: DOI: 10.1002/ange.201604158
Internationale Ausgabe: DOI: 10.1002/anie.201604158

Na_3SbS_4: A Solution Processable Sodium Superionic Conductor for All-Solid-State Sodium-Ion Batteries

Abhik Banerjee[+], Kern Ho Park[+], Jongwook W. Heo, Young Jin Nam, Chang Ki Moon, Seung M. Oh, Seung-Tae Hong, and Yoon Seok Jung**

Abstract: *All-solid-state sodium-ion batteries that operate at room temperature are attractive candidates for use in large-scale energy storage systems. However, materials innovation in solid electrolytes is imperative to fulfill multiple requirements, including high conductivity, functional synthesis protocols for achieving intimate ionic contact with active materials, and air stability. A new, highly conductive (1.1 mS cm^{-1} at 25 °C, $E_a = 0.20$ eV) and dry air stable sodium superionic conductor, tetragonal Na_3SbS_4, is described. Importantly, Na_3SbS_4 can be prepared by scalable solution processes using methanol or water, and it exhibits high conductivities of 0.1–0.3 mS cm^{-1}. The solution-processed, highly conductive solidified Na_3SbS_4 electrolyte coated on an active material ($NaCrO_2$) demonstrates dramatically improved electrochemical performance in all-solid-state batteries.*

The provision of stable electricity from renewable energy sources requires large-scale energy storage systems (ESSs).[1] Sodium-ion batteries (NIBs) are more competitive for application in ESSs than lithium-ion batteries (LIBs) in terms of their cost and environmental effect.[1b,c,2] Moreover, solidification of electrolytes in batteries avoids serious safety concerns, such as flammability and leakage, thereby guaranteeing the reliability of ESSs.[3] In this regard, all-solid-state sodium-ion batteries (ASNBs) are good candidates for use in ESSs.[3b] In particular, composite-structured bulk-type all-solid-state batteries are promising because of their scalable fabrication and high energy density.[3,4]

Among various solid electrolyte (SE) candidates, sulfide rather than oxide materials are the key to success for bulk-type all-solid-state batteries.[3,4] Sulfide SEs exhibit high conductivity, as found in several state-of-the-art sulfide lithium-ion SEs with conductivities comparable to that of liquid electrolytes (for example, $Li_{10}GeP_2S_{12}$ (12 mS cm^{-1}), $Li_7P_3S_{11}$ (17 mS cm^{-1})).[3a,5] Additionally, sulfide materials are deformable and consequently two-dimensional (2D) contact with active materials can be made by simple cold-pressing.[4a,6] Despite these advantages, several challenges remain before the widespread use of SEs may be accomplished.

First, composite electrodes in bulk-type all-solid-state batteries suffer from poor ionic contact.[6b,7] In conventional fabrication of composite electrodes, the SE powders are physically mixed with active materials and the powder mixtures are subsequently subjected to cold-pressing.[3,4] Despite the deformability of sulfide SE materials, cold-pressing alone is not enough to form void-free dense composites.[4a,6b,7] Additionally, the mixing of heterogeneous solid particles results in aggregation of each component.[4a,6b,7] As a consequence, bulk-type all-solid-state systems employing highly conductive SEs have performed below par.[3c,4a] As long as preparation of SEs relies on conventional synthesis protocols, such as solid-state reactions at high temperatures, no breakthrough in achieving intimate ionic contact is expected.[3c,4a,7] Second, the primary disadvantage of sulfide materials is their instability in air.[3c,4a,8] Recently, our group reported the fabrication of a novel lithium superionic conductor, $0.4\,LiI{\cdot}0.6\,Li_4SnS_4$, which showed high conductivity (0.41 mS cm^{-1}), stability in dry air, and solution processability using methanol (MeOH). This conductor, in the form of SE-coated $LiCoO_2$, demonstrated outstanding performance in conjunction with all-solid-state lithium-ion batteries.[4a] Our search for novel SE materials capable of tackling multiple issues at the same time has thus been expanded to sodium-ion SEs and ASNBs.

The search for sulfide sodium superionic conductors was initiated by the development of cubic Na_3PS_4 (NPS), which showed a conductivity of 0.46 mS cm^{-1}, a value that is much higher than that of the tetragonal phase.[3b,9] By forming a solid solution with Na_4SiS_4 ($94\,Na_3PS_4{\cdot}6\,Na_4SiS_4$), the conductivity of NPS was further increased to 0.74 mS cm^{-1}.[10] An even higher conductivity of 1.16 mS cm^{-1} was achieved by replacing sulfur in NPS with selenium (Na_3PSe_4). This enhancement is explained by lattice expansion while retaining the same cubic structure and the presence of highly polarizable selenium.[11] It was anticipated that Na_3SbS_4 might also show high conductivity considering the similar size of SbS_4^{3-} with respect to PSe_4^{3-}.[12] Very recently, another type of sodium-ion conductor was reported, $Na_{10}SnP_2S_{12}$, which showed a conductivity of 0.4 mS cm^{-1}.[13] Overall, only a few sulfide sodium-ion SEs have been developed. Thus, there is much room for further improvement in composition and structure by design of materials. Moreover, important

[*] Dr. A. Banerjee,[+] K. H. Park,[+] Y. J. Nam, C. K. Moon, Prof. Y. S. Jung
School of Energy and Chemical Engineering
Department of Energy Engineering, UNIST
Ulsan 44919 (South Korea)
E-mail: ysjung@unist.ac.kr
K. H. Park,[+] Prof. S. M. Oh
School of Chemical and Biological Engineering
Seoul National University
Seoul 151-742 (South Korea)
J. W. Heo, Prof. S.-T. Hong
Department of Energy Systems Engineering, DGIST
Daegu 42988 (South Korea)
E-mail: st.hong@dgist.ac.kr
[+] These authors contributed equally to this work.

Supporting information for this article can be found under: http://dx.doi.org/10.1002/anie.201604158.

considerations other than conductivity have not been scrutinized yet. The previously developed sulfide sodium-ion SE materials were based on phosphorus, which has a high affinity with oxygen, and consequently they were not stable in air.[4a] Importantly, no solution processable sulfide sodium-ion SE materials are known, which is related to the unavailability of solvents that can dissolve SEs without irreversible or side reactions.[7]

Herein, we report the synthesis of a new type of sodium superionic conductor, Na_3SbS_4. Na_3SbS_4 has a tetragonal structure with three-dimensional (3D) sodium ion diffusion channels. It exhibits a high ionic conductivity of 1.1 mS cm^{-1} at 25 °C and a low activation energy of 0.20 eV. More importantly, for the first time, solution-processing for sodium-ion SEs is demonstrated. Na_3SbS_4 prepared from MeOH or aqueous solutions exhibits high ionic conductivities of 0.1–0.3 mS cm^{-1}. The solution-processed solidified 13 wt % Na_3SbS_4 coating on $NaCrO_2$ (NCO) provides intimate ionic contact and well-percolated SEs, resulting in dramatic improvement in the utilization of NCO for these electrodes in all-solid-state cells over conventional mixed electrodes.

For the solid-state synthesis, Na_3SbS_4 powders were prepared from a stoichiometric mixture of Na_2S, Sb_2S_3, and sulfur powders at 550 °C. Figure 1 a presents the powder X-ray Rietveld refinement profile for Na_3SbS_4. All the peaks could be indexed to the tetragonal structure ($a = 7.1453$ Å and $c = 7.2770$ Å, $Z = 2$, $P\bar{4}2_1c$, no.114; Supporting Information, Tables S1 and S2) without any noticeable impurities,[14] which is isostructural with tetragonal Na_3PS_4[15] and slightly elongated from previously reported cubic Na_3SbS_4.[16] The unit cell structure consists of a body-centered tetragonal sublattice of SbS_4^{3-} tetrahedra that are connected to neighboring tetrahedra by sodium ions (Figure 1 b; Supporting Information, Figure S1–3). The presence of SbS_4^{3-} was also confirmed from three distinct peaks in the Raman spectrum (Supporting Information, Figure S4).[17] In the [010] view (Figure 1 b), sodium ion diffusion channels are apparently seen perpendicular to the plane. It should be noted that such channels exist parallel to all three crystallographic axes (Figure 1 b; Supporting Information, Figure S1) to form orthogonal 3D networks (Supporting Information, Figure S2). For a better understanding of the sodium ion conduction pathways of Na_3SbS_4, the bond valence sum mapping (BVSM) method was utilized.[18] Figure 1 c shows the BVS isosurfaces at ±0.3 v.u., clearly demonstrating the 3D network of the sodium ion conduction pathways along the *a*- (or *b*-) and *c*-axes, which implies the high ionic conductivity of Na_3SbS_4. It is also noted that the channels appear to have a bottleneck along the *c*-axis, as indicated by the narrower isosurfaces between the sodium ions than in the *a*-*b* plane (see the Supporting Information, Figure S5), which might reflect preferential 2D conduction.

The electronic conductivity of Na_3SbS_4 measured by the four probe method[19] was less than 10^{-8} S cm^{-1}. The electrical conductivity of Na_3SbS_4 measured by the AC impedance method using sodium ion blocking cells, which is in turn interpreted as ionic conductivity, is shown in Figure 2 and Table 1 (typical Nyquist plots are shown in the Supporting Information, Figure S6). Tetragonal Na_3SbS_4 possesses a conductivity value of 1.1 mS cm^{-1} at 25 °C and an activation energy of 0.20 eV, which is comparable to the best result obtained to date for cubic Na_3PSe_4 (Supporting Information, Table S3).[11] The high conductivity of Na_3SbS_4 is attributed to an open framework with 3D sodium ion channels (Figures 1 b and 1 c; Supporting Information, Figures S1 and S5).[20] A trace amount of sodium vacancies may also contribute to the high conductivity of Na_3SbS_4, although precise determination of the amount was beyond the experimental limits of X-ray refinement.[12]

The dry air stability of Na_3SbS_4 was tested by exposing the SE powders to a flow of dry air for 24 h. After the exposure, only marginal degradation in conductivity and the same activation energy were observed (Figure 2). Furthermore, the XRD pattern of Na_3SbS_4 after exposure to dry air did not

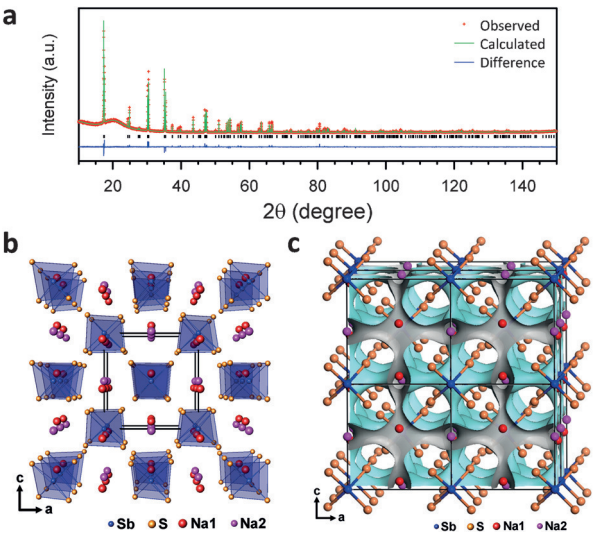

Figure 1. Structural analysis results of Na_3SbS_4. a) X-ray Rietveld refinement profile for the Na_3SbS_4 powders recorded at room temperature. b) Crystal structure of Na_3SbS_4 with the unit cell outlined. c) 3D bond valence map isosurfaces for Na_3SbS_4 with an isovalue of ±0.3 v.u.

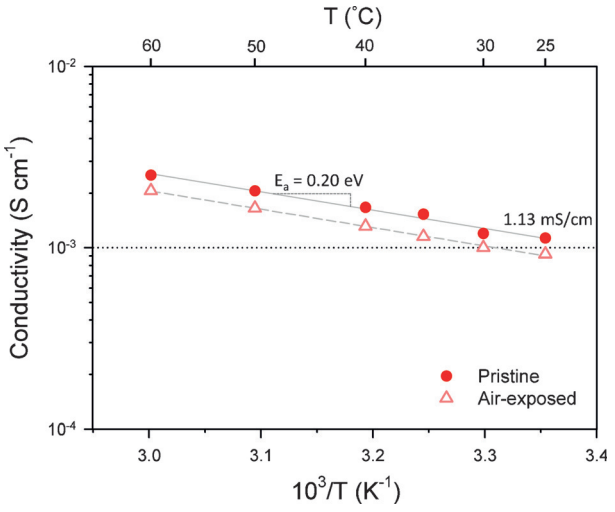

Figure 2. Conductivity of Na_3SbS_4 prepared by solid-state reaction at 550 °C. Data after exposure to dry air for 24 h is also compared.

Table 1: Conductivity and activation energy values for Na_3SbS_4 prepared by solid-state reaction and the solution process using MeOH or H_2O.

Sample	Preparation	Temperature[a] [°C]	σ_{25} [mS cm^{-1}]	E_a [eV]
Na_3SbS_4	Solid-state	550	1.1	0.20
NSbS-M100	MeOH	100	0.23	0.37
NSbS-M200	MeOH	200	0.11	0.38
NSbS-W100	H_2O	100	0.26	0.32
NSbS-W200	H_2O	200	0.15	0.30

[a] Heat-treatment temperature.

differ from that before exposure (Supporting Information, Figure S7a), indicating that the material possesses good stability. In sharp contrast, the XRD pattern of NPS showed a noticeable unknown broad peak ("*" in the Supporting Information, Figure S7b) after exposure to dry air. Accordingly, the conductivity value decreased by approximately one order of magnitude (from 0.11 to 0.02 mS cm^{-1}), confirming the instability of NPS in dry air. According to hard and soft acid and base (HSAB) theory, antimony (a softer acid than phosphorus) demonstrates reduced affinity for oxygen (a hard base), which explains the superior stability of Na_3SbS_4 in dry air compared to NPS.[4a,7,8] However, Na_3SbS_4 appeared to change after 48 h of exposure to ambient air, forming a hydrated compound ($Na_3SbS_4 \cdot 9\,H_2O$; Supporting Information, Figure S8a). Interestingly, Na_3SbS_4, with a conductivity of 0.34 mS cm^{-1}, was recovered by heat treatment of the hydrated form under vacuum at 200 °C (Supporting Information, Figures S8b,c). Na_3SbS_4 also showed moderate stability upon exposure to CO_2 (Supporting Information, Figure S9). After exposure to a flow of CO_2 for 24 h, no noticeable change in the XRD pattern (Supporting Information, Figure S9b) and only a slight decrease in conductivity (0.82 mS cm^{-1}) were observed.

Importantly, Na_3SbS_4 showed excellent solubility in water and MeOH, from which solidification of the dissolved solutions was attempted. After forming yellowish homogeneous solutions by dissolving the Na_3SbS_4 powders in MeOH or water, the solvents were removed by drying under vacuum at room temperature, followed by heat treatment under vacuum (Supporting Information, Figure S10). The results for MeOH and aqueous solution processes are shown in Figure 3 and Figure S11 (Supporting Information), respectively. Hereafter, the MeOH and aqueous solution-processed samples heat-treated at a given temperature (°C) are referred to as "**NSbS-Mx**" and "**NSbS-Wx**". Further consideration of the application of the solution process to SE coating on active materials suggests that a minimum temperature at which the solvents can be removed would be desirable to avoid any reaction between the electrode materials and the coated SEs. From thermogravimetric analysis (TGA) results (Figure 3b; Supporting Information, Figure S11b), heat-treatment temperatures of 100, 150, and 200 °C were thus selected.

In all solution-processed samples, XRD patterns identical to that for solid-state synthesized Na_3SbS_4 were observed, but with broadened peaks (Figures 1 and 3c; Supporting Information, Figure S11c). The Raman spectra for the solution-processed samples also clearly showed strong signatures for

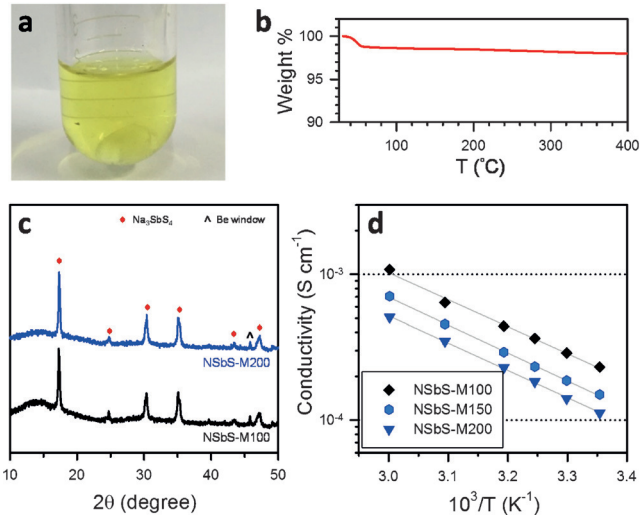

Figure 3. Preparation and characterization of solution processable Na_3SbS_4. a) Photograph of Na_3SbS_4 dissolved in MeOH solution. b) TGA profile for the Na_3SbS_4 xMeOH powders obtained by drying under vacuum at room temperature. c) XRD patterns and d) conductivities of Na_3SbS_4 processed in MeOH solution and prepared at different heat-treatment temperatures.

SbS_4^{3-} (Supporting Information, Figure S12).[17] However, the samples heat-treated at 200 °C (**NSbS-M200** and **NSbS-W200**) exhibited additional broad peaks at approximately 320–220 cm^{-1} (Supporting Information, Figures S12a,b). This might be related to the formation of trace amounts of surface impurities such as Sb_2S_3 or Sb_2S_5 (Supporting Information, Figure S12c).[21] Importantly, high conductivity values of 0.1–0.3 mS cm^{-1} were achieved for all MeOH and aqueous solution-processed Na_3SbS_4 (Figure 3d, Table 1; Supporting Information, Figure S11d). The lower conductivities and higher activation energies for solution-processed Na_3SbS_4, compared to solid-state synthesized Na_3SbS_4, are the result of the low heat-treatment temperatures, which led to lowered crystallinity and/or to the formation of surface impurities. It is expected that further increases in conductivity may be possible by iso-/aliovalent substitution or by the addition of NaX (X: Cl, Br, I) for both solid-state synthesized and solution processable Na_3SbS_4, as demonstrated for lithium-ion SE materials such as Li_4SnS_4.[4a,8]

Finally, a solution-processed coating of highly conductive Na_3SbS_4 was adopted on an electrode material, NCO ($NaCrO_2$). NCO was chosen because of its excellent reversibility for sodiation–desodiation, simple preparation method, and thermal stability.[2] NCO showed normal electrochemical behavior in liquid-electrolyte cells (Supporting Information, Figure S13).[2] The solution-processed coating of Na_3SbS_4 on NCO was carried out by following the same MeOH solution process in the presence of NCO powders at a heat-treatment temperature of 200 °C. The MeOH solution process was applied because NCO is not stable in water.[2,22] A moderate quality of Na_3SbS_4 coating on NCO is observed in electron microscopy images (Figures 4a,b; Supporting Information, Figures S14–16). In the high-resolution transmission electron microscopy (HRTEM) image of a focused ion beam (FIB) cross-sectioned Na_3SbS_4-coated NCO and its corresponding

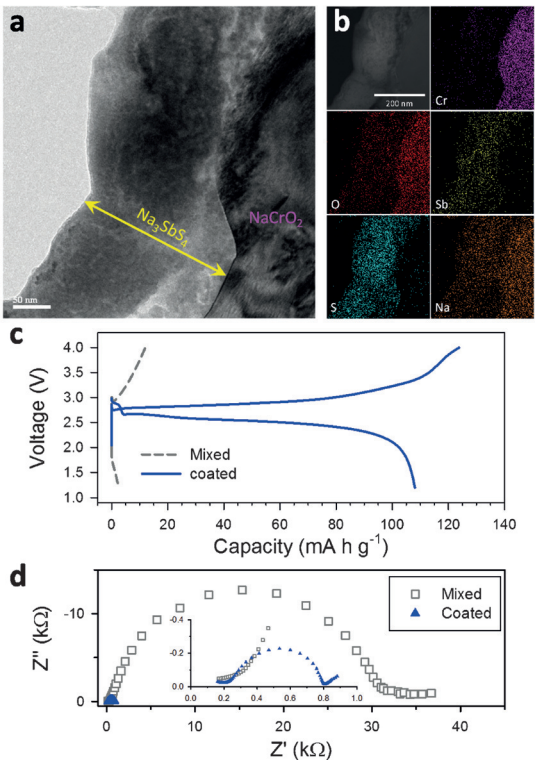

Figure 4. Results of Na_3SbS_4-coated $NaCrO_2$ (NCO). a) HRTEM image of FIB-sectioned Na_3SbS_4-coated NCO. b) Annular dark-field (ADF) TEM image of FIB-sectioned Na_3SbS_4-coated NCO and its corresponding EDXS elemental maps. c) Initial charge–discharge voltage profiles (50 μA cm^{-2}, 30 °C). d) Nyquist plots of NCO/Na-Sn all-solid-state cells. Results of the mixed electrode and the Na_3SbS_4-coated NCO electrode are compared. The cells were fabricated by pressing at 370 MPa. The NCO:Na_3SbS_4 weight ratio is 87:13.

energy dispersive X-ray spectroscopy (EDXS) elemental maps (Figures 4a,b), an approximately 200 nm thick coating of Na_3SbS_4 on NCO is clearly seen. Improvement of quality of the Na_3SbS_4 coating, in terms of uniformity and surface coverage, may be possible by elaborating the experimental conditions for the solution process or by applying a spray-coating method.[3a,23] The selected area electron diffraction (SAED) pattern for the Na_3SbS_4 coating (Supporting Information, Figure S16) also agrees well with the XRD results (Figure 3c).

The electrochemical performance of all-solid-state NCO/Na–Sn cells using the as-prepared Na_3SbS_4-coated NCO was compared to that using a conventional mixed electrode. The weight fraction of SE (Na_3SbS_4) was 13 wt%. For the mixed electrode, Na_3SbS_4 prepared by solid-state synthesis with a conductivity of 1.1 mS cm^{-1} was used. No carbon additives were included in the electrodes, thus providing a simple system to investigate the effects of the SE coating.[4a] Figure 4c displays the initial charge–discharge voltage profiles at 50 μA cm^{-2} at 30 °C. The mixed electrode shows a negligible discharge capacity. The applied pressure used to fabricate the cells with the mixed electrodes may be increased from 370 to 590 MPa, resulting in an increase of discharge capacity from 3 to 11 mA h g^{-1} (Figure 4c; Supporting Information, Figure S17), implying the importance of ionic contact. Surprisingly, the Na_3SbS_4-coated NCO shows a discharge capacity of 108 mA h g^{-1}, which is almost the same value as that for the liquid-electrolyte cell (Supporting Information, Figure S13b). A slight increase in the weight fraction of SE to 15 wt% also resulted in a high capacity value of 104 mA h g^{-1} (Supporting Information, Figure S18a). The Nyquist plots in Figure 4d show that the amplitude of the semicircle for the mixed electrode (corresponding to the charge transfer resistance at the SE–NCO interface)[4a,24] is huge, ($\approx$30 kΩ) in contrast to approximately 0.6 kΩ for the coated electrode.

Considering that the conductivity of Na_3SbS_4 (1.1 mS cm^{-1}) used in the mixed electrode is one order of magnitude higher than that for **NSbS-M200** (0.11 mS cm^{-1}) with an SE-coated electrode, it is striking that the SE-coated NCO electrode dramatically outperforms the mixed electrode. This result is in line with our previous findings for 0.4 LiI·0.6 Li_4SnS_4-coated $LiCoO_2$ for all-solid-state lithium-ion batteries.[4a] The electrode from $LiCoO_2$ coated by 0.4 LiI·0.6 Li_4SnS_4 (0.41 mS cm^{-1}) outperformed the mixed electrodes employing the same SE (0.4 LiI·0.6 Li_4SnS_4) or $Li_{10}GeP_2S_{12}$ (6.0 mS cm^{-1}).[4a] Voltage profiles for the conventional mixed electrode using NPS showing the same conductivity (0.11 mS cm^{-1}) as the solution-processed Na_3SbS_4 (**NSbS-M200**) were also compared (Supporting Information, Figure S18b). The NPS mixed electrode exhibits much higher overpotential and a correspondingly lowered capacity (94 mA h g^{-1}) than the Na_3SbS_4-coated electrode. To clarify the origin of the dramatic improvement in performance of the coated electrodes, compared to the mixed electrodes, electron microscopy analysis on composite structures was carried out. The field emission scanning electron microscopy (FESEM) images and their corresponding EDXS elemental maps for the electrode surfaces (Supporting Information, Figure S19) and cross-sections (Supporting Information, Figures S20 and S21) were compared with the Na_3SbS_4-coated NCO electrode and the mixed electrode: 1) a much more uniform spatial distribution of SEs and active materials is confirmed for the coated electrode when compared to the mixed electrode; 2) and for the coated electrode, the SE fills the voids between the NCO particles to form intimate contacts. In stark contrast, many voids are evident for the mixed electrode between the NCO particles with the segregated SE regions. These observations imply far superior ionic conduction and ionic contacts in the SE-coated electrode compared to that of the mixed electrode, thus explaining the significantly improved electrochemical performances. Overall, the combined results demonstrate the exceptional advantages of solution processable SE, Na_3SbS_4, as a means to satisfy the challenging requirements of all-solid-state batteries, intimate ionic contact, and uniform spatial distribution of SEs.

Unfortunately, the NCO/Na–Sn all-solid-state cell using Na_3SbS_4-coated NCO showed gradual capacity fading upon repeated cycling (Supporting Information, Figure S22), which could be explained by poor electrochemical stability of sulfide SEs,[3c,24] chemical reaction between NCO and Na_3SbS_4,[25] a space charge layer model,[26] and lattice mismatch.[26] It should be noted that the results in this work were obtained using NCO powders without any protective coatings. Further improvements of the electrochemical performances could be

possible by protective coating on cathode material (NCO) as demonstrated for surface-modified $LiCoO_2$ in all-solid-state lithium-ion batteries.[3a,c,4a,5c,6]

In summary, a high conductivity of 1.1 mS cm^{-1}, good stability in dry air, and scalable solution processability using MeOH or water, were successfully demonstrated for a new sodium superionic conductor, tetragonal Na_3SbS_4. The structural refinement revealed 3D sodium ion diffusion channels, with a preference for 2D diffusion in the *a-b* plane. Finally, the high conductivity (0.1 mS cm^{-1}), intimate ionic contact with the active material, and well-percolated SEs enabled by the solution-processed Na_3SbS_4, resulted in a dramatically improved electrochemical performance of NCO/Na-Sn ASNBs. We believe that our results will ignite interest in materials design and synthesis for superionic conductors and advance commercialization of all-solid-state technologies.

Acknowledgements

This work was supported by Basic Science Research Program through the National Research Foundation of Korea (NRF) funded by the Ministry of Education (No. NRF-2014R1A1A2058760) and by the 2016 Research Fund (1.160004.01) of UNIST.

Keywords: batteries · chalcogens · sodium · solid electrolytes · solution process

How to cite: *Angew. Chem. Int. Ed.* **2016**, *55*, 9634–9638
Angew. Chem. **2016**, *128*, 9786–9790

[1] a) J. B. Goodenough, Y. Kim, *Chem. Mater.* **2010**, *22*, 587–603; b) J.-M. Tarascon, *Philos. Trans. R. Soc. London Ser. A* **2010**, *368*, 3227–3241; c) B. Dunn, H. Kamath, J.-M. Tarascon, *Science* **2011**, *334*, 928–935.

[2] a) S. Y. Hong, Y. Kim, Y. Park, A. Choi, N.-S. Choi, K. T. Lee, *Energy Environ. Sci.* **2013**, *6*, 2067–2081; b) N. Yabuuchi, K. Kubota, M. Dahbi, S. Komaba, *Chem. Rev.* **2014**, *114*, 11636–11682.

[3] a) N. Kamaya, K. Homma, Y. Yamakawa, M. Hirayama, R. Kanno, M. Yonemura, T. Kamiyama, Y. Kato, S. Hama, K. Kawamoto, A. Mitsui, *Nat. Mater.* **2011**, *10*, 682–686; b) A. Hayashi, K. Noi, A. Sakuda, M. Tatsumisago, *Nat. Commun.* **2012**, *3*, 856; c) Y. S. Jung, D. Y. Oh, Y. J. Nam, K. H. Park, *Isr. J. Chem.* **2015**, *55*, 472.

[4] a) K. H. Park, D. Y. Oh, Y. E. Choi, Y. J. Nam, L. Han, J.-Y. Kim, H. Xin, F. Lin, S. M. Oh, Y. S. Jung, *Adv. Mater.* **2016**, *28*, 1874–1883; b) T. A. Yersak, H. A. Macpherson, S. C. Kim, V. D. Le, C. S. Kang, S. B. Son, Y. H. Kim, J. E. Trefvey, K. H. Oh, C. Stoldt, S. H. Lee, *Adv. Energy Mater.* **2013**, *3*, 120–127.

[5] a) Y. Seino, T. Ota, K. Takada, A. Hayashi, M. Tatsumisago, *Energy Environ. Sci.* **2014**, *7*, 627–631; b) Y. Wang, W. D. Richards, S. P. Ong, L. J. Miara, J. C. Kim, Y. Mo, G. Ceder, *Nat. Mater.* **2015**, *14*, 1026; c) Y. Kato, S. Hori, T. Saito, K. Suzuki, M. Hirayama, A. Mitsui, M. Yonemura, H. Iba, R. Kanno, *Nat. Energy* **2016**, DOI: 10.1038/nenergy.2016.1030; d) J. Maier, *Nat. Mater.* **2005**, *4*, 805–815.

[6] a) A. Sakuda, A. Hayashi, M. Tatsumisago, *Sci. Rep.* **2013**, *3*, 2261; b) Y. J. Nam, S. J. Jo, D. Y. Oh, J. M. Im, S. Y. Kim, J. H. Song, Y. G. Lee, S. Y. Lee, Y. S. Jung, *Nano Lett.* **2015**, *15*, 3317.

[7] D. Y. Oh, Y. J. Nam, K. H. Park, S. H. Jung, S.-J. Cho, Y. K. Kim, Y.-G. Lee, S.-Y. Lee, Y. S. Jung, *Adv. Energy Mater.* **2015**, *5*, 1500865.

[8] G. Sahu, Z. Lin, J. Li, Z. Liu, N. Dudney, C. Liang, *Energy Environ. Sci.* **2014**, *7*, 1053–1058.

[9] A. Hayashi, K. Noi, N. Tanibata, M. Nagao, M. Tatsumisago, *J. Power Sources* **2014**, *258*, 420–423.

[10] N. Tanibata, K. Noi, A. Hayashi, M. Tatsumisago, *RSC Adv.* **2014**, *4*, 17120–17123.

[11] L. Zhang, K. Yang, J. Mi, L. Lu, L. Zhao, L. Wang, Y. Li, H. Zeng, *Adv. Energy Mater.* **2015**, *5*, 1501294.

[12] S.-H. Bo, Y. Wang, J. C. Kim, W. D. Richards, G. Ceder, *Chem. Mater.* **2016**, *28*, 252–258.

[13] W. D. Richards, T. Tsujimura, L. J. Miara, Y. Wang, J. C. Kim, S. P. Ong, I. Uechi, N. Suzuki, G. Ceder, *Nat. Commun.* **2016**, *7*, 11009.

[14] Further details of the crystal structure investigation may be obtained from the Fachinformationszentrum Karlsruhe, 76344 Eggenstein-Leopoldshafen, Germany (fax: (+76349) 77247-76808-76666; e-mail: crysdata@fiz-karlsruhe.de), on quoting the depository number CSD 431205.

[15] M. Jansen, U. Henseler, *J. Solid State Chem.* **1992**, *99*, 110–119.

[16] H. A. Graf, H. Schafer, *Z. Anorg. Allg. Chem.* **1976**, *425*, 67–80.

[17] W. Mikenda, A. Preisinger, *Spectrochim. Acta Part A* **1980**, *36*, 365–370.

[18] M. Sale, M. Avdeev, *J. Appl. Crystallogr.* **2012**, *45*, 1054–1056.

[19] Y. S. Jung, A. S. Cavanagh, L. A. Riley, S. H. Kang, A. C. Dillon, M. D. Groner, S. M. George, S. H. Lee, *Adv. Mater.* **2010**, *22*, 2172–2176.

[20] P. G. Bruce, *Solid state electrochemistry*, Cambridge University Press, Cambridge, **1995**.

[21] a) G. G. Long, L. H. Bowen, *Inorg. Nucl. Chem. Lett.* **1970**, *6*, 837–842; b) B. H. Juarez, S. Rubio, J. Sanchez-Dehesa, C. Lopez, *Adv. Mater.* **2002**, *14*, 1486–1490.

[22] C.-Y. Yu, J.-S. Park, H.-G. Jung, K.-Y. Chung, D. Aurbach, Y.-K. Sun, S.-T. Myung, *Energy Environ. Sci.* **2015**, *8*, 2019–2026.

[23] N. Ohta, K. Takada, I. Sakaguchi, L. Zhang, R. Ma, K. Fukuda, M. Osada, T. Sasaki, *Electrochem. Commun.* **2007**, *9*, 1486–1490.

[24] B. R. Shin, Y. J. Nam, D. Y. Oh, D. H. Kim, J. W. Kim, Y. S. Jung, *Electrochim. Acta* **2014**, *146*, 395–402.

[25] A. Sakuda, A. Hayashi, M. Tatsumisago, *Chem. Mater.* **2010**, *22*, 949–956.

[26] J. Haruyama, K. Sodeyama, L. Han, K. Takada, Y. Tateyama, *Chem. Mater.* **2014**, *26*, 4248–4255.

Received: April 28, 2016
Revised: June 2, 2016
Published online: July 5, 2016

